The Effect of Amino Acids on the Fenton and photo-Fenton Reactions in Cloud Water: Unraveling the Dual Role of Glutamic Acid

Peng Cheng [1,2], Gilles Mailhot [1,3], Mohamed Sarakha [1], Guillaume. Voyard [1], Daniele Scheres Firak [4], Thomas Schaefer [4], Hartmut Herrmann [4], Marcello Brigante [1]*

[1] Université Clermont Auvergne, CNRS, Institut de Chimie de Clermont-Ferrand, F-63000 Clermont–Ferrand, France.

[2] Department of Environmental Engineering, School of Resources and Environmental Science, Wuhan University, 430079, PR China

[3] Université Clermont Auvergne, CNRS, Laboratoire de Météorologie Physique (LaMP), F-63000 Clermont–Ferrand, France.

[4] Atmospheric Chemistry Department (ACD), Leibniz- Institute for Tropospheric Research (TROPOS), 04318 Leipzig, Germany

*Corresponding author:

Marcello Brigante (Marcello.Brigante@uca.fr)

ABSTRACT

In this work, Glutamic acid (Glu) was selected as a model amino acid (AAs) to investigate its complexation with Fe(III) and Fe(II), focusing on its impact on the Fenton reaction and the photolysis of Fe(III) in cloud aqueous phase. Glu was found to enhance the rate constant for the reaction of Fe(II)-Glu with H_2O_2 to $1.54\pm0.13\times10^4$ M^{-1} s^{-1}, which is significantly higher than that of classic Fenton reactions (~50-70 M^{-1} s^{-1}). In contrast, the photolysis quantum yield of Fe(III)-Glu complex was determined to be 0.037 under solar simulated irradiation, largely lower than Fe(III)-hydroxy complexes (0.216). In the overall process (Fenton or Fe(III) photolysis), it was found that $^{\bullet}OH$ formation decreased in the presence of Glu. Additionally, the fate of Glu in the presence of Fe(III) was investigated as well as the oxidation process (driven by $^{\bullet}OH$ and ligand-to-metal charge transfer (LMCT) reaction) led to the formation of short-chain carboxylic acids and ammonium under simulated solar light. Interestingly, these two processes generated different primary short-chain carboxylic acids, indicating distinct mechanisms. This study provides valuable insights into the role and fate of amino acids in atmospheric chemistry, helping to further understand their impact on atmospheric processes.

SYNOPSIS

This study investigates the complexation of Fe(II) and Fe(III) with glutamic acid under cloud water conditions and the effect on Fenton and photo-Fenton reactions, hydroxyl radical formation, and their impact on amino acid oxidation.

1. INTRODUCTION

The Earth's atmosphere is a dynamic system in which different phases, including gases, aerosol particles, water droplets, and ice particles, are all engaged in complex chemical interactions that continually modify the atmospheric chemical composition (Bianco et al., 2020; Kanakidou et al., 2018). Among these, the cloud aqueous phase stands out as a critical reactive system, encompassing gaseous, liquid, and solid components. In recent years, intensified research efforts have centered on unraveling the composition of atmospheric cloud waters, significantly advancing our comprehension of multiphase chemistry within the atmosphere (Bianco et al., 2018). Common components identified in both aerosols and cloud water include inorganic ions, transition metal ions (TMI) such as iron (Angle et al., 2021; Bianco et al., 2017), and organic carbon (Battaglia Jr. et al., 2019), notably amino acids (AAs). However, the influence of AAs on iron redox chemistry and hydroxyl radical ($^\bullet$OH) production in cloud water remains insufficiently understood.

Recent investigations have unveiled the presence of reactive oxygen species (ROS) in viscous aerosol particles, highlighting their pronounced reactivity in such environments (Alpert et al., 2021; Edwards et al., 2022). Hydroxy radicals ($^\bullet$OH) emerge as primary ROS in the atmospheric water phase, with concentrations estimated between 10^{-14} to 10^{-12} M^{-1} (Bianco et al., 2020; Gligorovski et al., 2015). Key sources of $^\bullet$OH include gas-droplet partitioning and in situ formation through processes like photolysis at surfaces or in the bulk phase, such as the photolysis of TMI and hydrogen peroxide (H_2O_2) (Bianco et al., 2015; Tilgner et al., 2013). Iron (Fe), copper (Cu), and manganese (Mn) have gained prominence as pivotal metals in atmospheric chemical processes due to their elevated concentrations, with Fe averaging around 10^{-6} M in the atmospheric aqueous phase (Sorooshian et al., 2013). Experimental evidence and

65   literature emphasize the crucial role of iron, particularly via (photo)-Fenton and (photo)-Fenton-

66   like processes, in the generation and budgeting of $^\bullet OH$ (R1-R5) (Guo et al., 2014; Tilgner et al.,

67   2013).

68    $$[Fe(H_2O)_6]^{3+} \xrightarrow{hv} [Fe(H_2O)_5]^{2+} + H^+ + {}^\bullet OH \tag{R1}$$

69    $$[Fe(H_2O)_5OH]^{2+} \xrightarrow{hv} [Fe(H_2O)_5]^{2+} + {}^\bullet OH \tag{R2}$$

70    $$[Fe(H_2O)_5]^{2+} + H_2O_2 \rightarrow [Fe(H_2O)_5OH]^{2+} + {}^\bullet OH \tag{R3}$$

71    $$[Fe(H_2O)_6]^{3+} + H_2O_2 \rightarrow [Fe(H_2O)_5]^{2+} + HO_2{}^\bullet + H_2O + H^+ \tag{R4}$$

72    $$[Fe(H_2O)_5OH]^{2+} + H_2O_2 \rightarrow [Fe(H_2O)_5]^{2+} + HO_2{}^\bullet + H_2O \tag{R5}$$
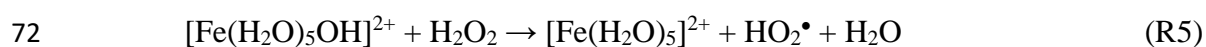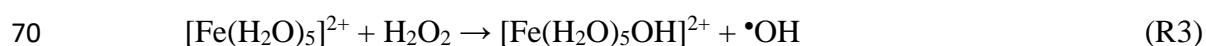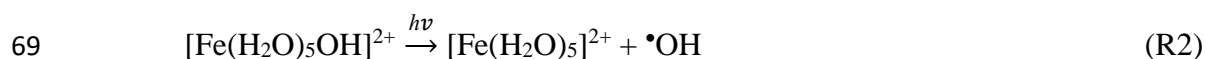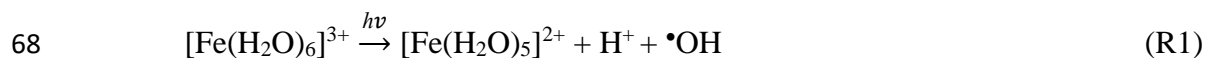
73   While Fe(III)/Fe(II) ions precipitate as oxides or hydroxides at pH higher than 4.0, in the cloud

74   water phase, iron complexes with organic ligands enhance stability under typical cloud water

75   photooxidation conditions (Soriano-Molina et al., 2018; Yuan et al., 2020). Various organic

76   ligands, including carboxylic acids and aldehydes, have been extensively studied (Long et al.,

77   2013; Marion et al., 2018; Soriano-Molina et al., 2018). However, less than 30 % of the

78   dissolved organic carbon (DOC) in the cloud-aqueous phase has been molecularly characterized,

79   with AAs constituting a significant portion of DOC (Bianco et al., 2016). Numerous field

80   studies have confirmed the presence of AAs in cloud water, rain, fog, and aerosols, with

81   concentrations typically ranging from low nanomolar to micromolar levels, depending on the

82   location and sampling method (Matos et al., 2016; van Pinxteren et al., 2023; Renard et al.,

83   2022; Triesch et al., 2021). For example, Renard et al. (2022) detected more than 15 AAs in

84   cloud water collected at Puy de Dôme, France, with glutamate being one of the most abundant

85   species. These compounds originate from both primary emissions (e.g., bioaerosols, ocean

86   spray) and secondary atmospheric processes (e.g., processing of proteins or peptides within

87   clouds) (Mace et al., 2003; Samy et al., 2011). Amino acids, as key nitrogen-containing

88   components in organic matter, can significantly affect the oxidation capacity of cloud water

89   through free radical scavenging and metal complexation reactions (Bianco et al., 2016; Marion

90   et al., 2018), but their specific atmospheric reactivity and transformation mechanisms are still

91   unclear. The photochemical behavior and fate of AAs in the atmosphere remain relatively

92   unexplored. For example, tryptophan can undergo direct photolysis, producing low-molecular-

93   weight compounds and dimerization products under solar-simulated conditions. Recent

94   investigations into the fate of the Fe(III)-aspartate complex demonstrate ligand-to-metal charge

95   transfer reactions (LMCT) and the formation of ammonia and short-chain carboxylic acids

96   (Marion et al., 2018).

97   However, the effect of the complexation between Fe(II) and AAs on the rate of Fenton reaction

98   and the yield of $^\bullet$OH in the atmosphere has not yet been investigated. Moreover, the effect of

99   the complexation between Fe(III) and AAs on the quantum yield of atmospheric photolysis of

100   Fe(III) deserves further investigation, since both processes highly affect the budget of $^\bullet$OH

101   during the day and night in the atmosphere. In addition, the complexation between Fe(III) and

102   AAs introduces two distinct photooxidation pathways: the photolysis of Fe-AAs complexes and

103   reactions between AAs and (photo)-generated $^\bullet$OH. Although both pathways significantly

104   contribute to the transformation of AAs in cloud water and impact inorganic and organic

105   chemical compositions, their mechanisms still lack further study, especially in terms of products

106   generation.

107   This study specifically focuses on glutamic acid (Glu), an AA regularly detected in cloud water

108   and aerosols (van Pinxteren et al., 2012; Triesch et al., 2021), and on the investigation of its

109   impact on iron (Fe(II)/Fe(III)) reactivity. The study explored i) the effect of Glu on the rate and

110   •OH yield of the Fenton reaction; and ii) the effect of Glu on the •OH production and Fe(II)

111   quantum yield during the Fe(III) photolysis. In addition, the study explores iii) two pathways

112   of Fe(III) and Fe(III)-Glu complex photolysis: the LMCT process and the reaction between Glu

113   and $^{\bullet}$OH, assessing their respective contributions to Glu fate. Utilizing competitive kinetic

114   experiments, the contributions of each pathway were estimated, and a detailed investigation of

115   the formation, and chemical mechanisms of transformation products was carried out. Ultimately,

116   our study aims to quantify the diverse contributions of different pathways in amino acid

117   conversion in the presence of iron.

118   **2. MATERIAL AND METHODS**

119   **2.1. Chemicals**

120   All chemicals were used without further purification: Fe(III)-perchlorate (99.9 %), Fe(II)-

121   perchlorate (99.9 %), L-glutamic acid monosodium salt (Glu, 99 %), hydrogen peroxide (H_2O_2,

122   30 %), malonic acid (99.0 %), and 2,4-dinitrophenylhydrazine (DNPH, 97 %) were purchase

123   from Sigma Aldrich. Sodium formate (99.0 %), potassium oxalate monohydrate (99.0 %),

124   sodium succinate dibasic (98.0 %), and 3-(2-pyridyl)-5,6-diphenyl-1,2,4-triazine-p, p'-sulfonic

125   acid monosodium salt hydrate (Ferrozine, 97 %) were purchased from Fluka. Ammonium

126   acetate (99.3 %) was purchased from Fisher. Water was purified using a reverse osmosis RIOS

127   5 and Synergy (Millipore) device (resistivity 18.2 MΩ cm, DOC < 0.1 mg L^{-1}). All solutions

128   were prepared in milli-Q water.

129   **2.2. Experimental procedure**

130   **2.2.1. Fenton reaction**

131   The Fenton experiments were carried out with Fe(II) perchlorate at room temperature and a pH

132   of 5.6 ± 0.1 (Kinetic experiments) and 3.8 ± 0.1 (Electron spin resonance (ESR) experiments).

133   The pH of 5.6 was chosen to favor the formation of Fe(II)-Glu complexes during the kinetic

134   studies, while the lower pH of 3.8 was selected for ESR experiments, as $^\bullet$OH detection by ESR

135   is more effective under acidic conditions. These two pH values fall within the typical range

136   observed in atmospheric cloud water. Specifically, pH of 3.8 represents more acidic conditions

137   often found in polluted regions, whereas pH of 5.6 reflects the composition of cloud water in

138   remote or less impacted environments (Pye et al., 2020; Shah et al., 2020). This range enables

139   the assessment of the system's behavior under environmentally relevant conditions.

140   The Fenton kinetic experiments were initiated by the addition of the H_2O_2 stock solution. Hence,

141   the designed H_2O_2 concentration are 100 and 25 μM in kinetics and ESR experiment

142   respectively. The solution was continuously stirred during the reaction. The pH of the solution

143   was adjusted using $HClO_4$ or NaOH solutions. The samples were taken every 15 seconds and

144   mixed with a solution of Ferrozine in phosphate buffer (pH = 7.0 ± 0.1) (Gabet et al., 2023).

145   Phenol was used as $^\bullet$OH scavenger in the experiment. As a scavenger, the required

146   concentration of phenol was calculated to quench $^\bullet$OH so that theoretically 99 % of $^\bullet$OH can be

147   trapped via reacting with phenol. The same method was used in the presence of Glutamic acid

148   (Glu) to study the Fe(II)-Glu complex Fenton-like reaction at the same pH. To get different

149   fractions of Fe(II)-Glu, Fe(II) was mixed with varying concentrations of Glu solution (0 - 25

150   mM) to calculate the rate constant of the Fenton reaction. The experimental data were analyzed

151   using Origin 2019 software. To determine and quantify the $^\bullet$OH generation in the Fenton

152   reaction, the ESR experiment was carried out using 5,5-dimethyl-1-pyrroline-N-oxide (DMPO)

153   as the spin trap. $Fe(ClO_4)_2$ and H_2O_2 were mixed with DMPO at a pH of 3.8 ± 0.1. The pH was

154   set because the ESR signal intensity was lower at a higher pH = 4.0. ESR spectroscopy was

155 performed on a Bruker EMX-plus spectrometer using the resonator 4119HS. Detailed

156 information was provided in the supplementary material section (**SM1**).

2.2.2. Photolysis of Fe(III)

158 To study the Fe(III) photolysis, isopropanol was used as a scavenger in the solution to quench

159 the generated $^{\bullet}OH$ radicals. The pH of the solution was adjusted to 3.8 ± 0.1 with $HClO_4$ or

160 NaOH solutions. The Fe(III) solution was irradiated in a Pyrex jacked cylindrical reactor (**Fig.**

161 **SM1**) with a circulation cooling system to keep a constant temperature of 283 ± 0.2 K. The

162 reactor was located at the focal point of a 500 W xenon lamp equipped with a Pyrex filter to

163 remove wavelengths < 290 nm and a water filter for infrared radiation absorption. The solution

164 was stirred with a Teflon-coated magnetic stirring bar to ensure homogeneity. The same setup

165 was used for the photolysis experiments in the presence of Fe(III)-Glu complexes. Different

166 fractions of Fe(III)-Glu were achieved by adding different amounts of a Glu 50 mM stock

167 solution (designed [Glu] = 0 - 200 μM).

168 The emission spectrum of the irradiation setup was recorded using a calibrated CCD camera

169 (Ocean Optics USB 2000+UV-Vis) coupled with an optical fiber. An irradiance of 8.38×10^3

170 $\mu W\ cm^{-2}$ was determined between 290 and 500 nm as shown in **Fig. SM2**. Compared to the

171 natural solar emission spectrum, the UV region between 290 and 400 nm, which contribute for

172 driving the photoreaction of Fe(III) and Fe(III)-Glu, shows a quite similar spectral profile, as

173 reported in our previous publication (Bianco et al., 2015). The Energy and photonic flux (I_0) of

174 the polychromatic irradiation at every nanometer wavelength are listed in **Table SM1**. Detailed

175 information about the calculation of the Fe(III) and Fe(III)-Glu photolysis quantum yield is

176 given in the supplementary material section (**SM2**). To quantify the $^{\bullet}OH$ generation during the

177 Fe(III) photolysis, isopropanol was used in excess (10 mM) as a selective $^{\bullet}OH$ probe.

178   Isopropanol reacts with $^\bullet$OH to form acetone which was quantified by HPLC (see section 2.4)

179   (Motohashi and Saito, 1993).

180   **2.2.3. Photodegradation of Glu**

181   To investigate the fate of Glu in various systems, experiments were performed using the

182   previously described photoreactor setup. Glu solutions, either alone or mixed with Fe(III)

183   and/or H_2O_2, were irradiated under simulated solar light at pH 3.8 ± 0.1. Samples were collected

184   at specific time intervals and analyzed using HPLC-MS (see section 2.4). To calculate and

185   compare the photodegradation kinetics of Glu in different systems, a pseudo-first-order kinetic

186   model was applied, expressed as Equation (1):

187            $-\ln(C_t/C_0) = k_{obs}\, t$ Eq (1)

188   where C_0 represents the initial concentration of Glu, and C_t is the concentration of Glu at time

189   t of irradiation. In addition, IC-MS and TOC analyses were performed to identify the generated

190   by-products and assess the mineralization of Glu (see section 2.4).

191   **2.3. Study of the speciation of the Fe(III)/Fe(II)-Glu complex**

192   The speciation of the Fe(III)/Fe(II)-Glu complex was studied using the Hyss 2009 software.

193   This analysis included the iron, iron-aqua, iron hydroxy, and iron-Glu complexes in the solution.

194   The parameters used in the software, such as iron and Glu concentrations, kept consistent with

195   the one in the experimental procedure. The stability constants (log K) used for the complexes,

196   such as the Fe(II)-Glu and Fe(III)-Glu complexes, etc. are listed in **Table SM2**. These constants

197   are derived from the Visual MINTEQ database or NIST database 46 and have been corrected

198   for a temperature of 25 °C and an ionic strength (I) of 0 M. The detailed method is provided in

199   the supplementary material section (**SM3**).

2.4. Chemical analysis

2.4.1. Fe(II), H$_2$O$_2$, and Acetone quantification

Iron (II) concentration was determined by using Ferrozine, which forms a stable magenta complex with Fe(II) (Fe(II)-ferrozine) (Gabet et al., 2023). Hydrogen peroxide concentration during experiments was determined by using a spectrofluorimetric quantification method (Bader et al., 1988). The concentration of generated acetone in the solution was evaluated by HPLC (Shimadzu NEXERA XR HPL) equipped with a photodiode array detector and an autosampler (Wang et al., 2005). **Fig. SM3** shows the calibration curve of Fe(II), H$_2$O$_2$, and acetone. More details are given in the supplementary material section (**SM4**).

2.4.2. UPLC-MS, IC-MS and TOC

The quantification of Glutamic acid (Glu) and the identification of its transformation products was conducted using a ThermoScientific Orbitrap Q-Exactive high-resolution mass spectrometry (HRMS) coupled with a ThermoScientific Ultimate 3000 RSLC ultra-high-performance liquid chromatography (UPLC) system. The quantification of carboxylic acid by-products and NH$_4^+$ resulting from Glu degradation was performed using a Thermo-Fisher Scientific ICS-6000 Ionic chromatograph interfaced with a simple quadrupole mass spectrometer (ISQ-EC-Thermo Scientific). The total organic carbon (TOC) concentration in the aqueous solution was followed by a Shimadzu TOC 5050A analyzer. Detailed information is reported in the Supplementary Material section (**SM5**).

2.5. Kinetic Modeling

To verify the obtained experimental rate constants of the reaction between Fe(II)-Glu and H$_2$O$_2$, COPASI software was utilized to simulate the kinetics of Fe(II) consumption and generation of

222 •OH in the Fenton reaction in the presence of Glu using the default settings of the deterministic

223 LSODA algorithm to solve ordinary differential equations (Hoops et al., 2006). The chemical

224 reactions considered in the model are provided in **Table SM3**. The majority of rate constants

225 used in the model were available in the literature or obtained from experimental results. For the

226 unknown or uncertain rate constants, the value is obtained from the estimation according to a

227 similar reaction.

3. RESULTS AND DISCUSSION

229 To investigate the effect of Glu on the Fe(II)/Fe(III) cycle, a complex set of experiments was

230 performed. First, the complexation of Fe(II)/Fe(III) with Glu was studied as a function of pH

231 and the initial concentration of Glu. Second, to study the effect of Glu on the Fenton reaction,

232 its rate constants and •OH generation in the presence of Glu were obtained experimentally and

233 using the kinetic model. The formation rates of Fe(II) and •OH were determined from Fe(III)

234 photolysis with or without Glu. Finally, the mechanism of Glu photo-transformation was

235 reported.

3.1. Complexation of Glu with Fe(II)/Fe(III)

237 The Fe speciation was initially investigated to understand how Glu interacts with iron ions

238 under various conditions with Hyss2009 software. **Fig. SM4a** shows the speciation of 20 μM

239 Fe(II) in the presence of Glu (0.2 – 25 mM) across a pH range of 4 to 10. It can be observed

240 that Fe(II) predominates until pH = 5, while the fraction of the Fe(II)-Glu complex increases

241 after this pH. Hence, a higher pH (5.6) was selected for the Fenton reaction to guarantee the

242 presence of complex, while still working under aerosol/cloud conditions and to avoid iron

243 precipitation occurring at higher pH values. At pH 5.6, the Fe(II)-Glu complex accounts for

244   2.2 % in the presence of 20 µM Fe(II) and 25 mM Glu. The complex fractions at varying Glu

245   concentrations at pH = 5.6 are provided in **Table SM4**.

246   **Fig. SM4b** shows the simulated speciation of Fe(III) (100 µM) as a function of pH in the

247   presence of Glu (10-20 µM). The Fe(III)-aqua, Fe(III)-hydroxy complexes, and Fe(III)-Glu

248   complexes were observed as a function of the pH. At pH = 3.8, [Fe(III)] = [Glu] = 100 µM, the

249   Fe(III)-hydroxy complexes $Fe(OH)^{2+}$ and $Fe(OH)_2^+$ represent 24.4 and 22.8 % of the total Fe(III)

250   concentration, respectively. In contrast, Fe(III)-Glu complex accounts for 52.3 % of the total

251   Fe(III), while Fe(III)-aqua complex constitutes only 0.5 %. The UV-Vis spectra of Fe(III), Glu,

252   and Fe(III)-Glu complex are depicted in **Fig. SM2**. The characteristic absorption band of Fe(III)

253   with a maximum at 297 nm, corresponding to the charge transfer bands of $Fe(OH)^{2+}$, becomes

254   attenuated in the presence of Glu. Moreover, the UV-Vis spectrum of Fe(III)-Glu mixture

255   differs from those of Fe(III) and Glu alone or the simple overlap of their individual spectra,

256   confirming the formation of a stable Fe(III)-Glu complex (Samavat et al., 2007). The fractions

257   of the generated complex in the presence of different Glu concentrations at pH = 3.8 are given

258   in **Table SM5**. For the sake of simplicity, Fe(III)/Fe(II)-hydroxy and Fe(III)/Fe(II)-aqua

259   complexes are hereafter referred as Fe(III) and Fe(II).

260   **3.2. Fenton reaction process in the presence of Glu**

261   **3.2.1. Fe(II) oxidation**

262   To study the effect of Glu on the kinetics of the Fenton reaction and determine the rate constant

263   of the reaction of Fe(II)-Glu with H_2O_2, experiments were performed using different

264   concentrations of Glu. **Fig. 1a** shows the faster Fe(II) concentration decreases when the Glu

265   concentration increases, which indicates that Glu can increase the reaction rate of Fe(II) with

266   H_2O_2. This is likely due to the formation of the Fe(II)-Glu complex which has a high reaction

267 rate constant with H_2O_2. As seen in **Fig. 1b**, the data obtained by plotting $\frac{-\frac{d[Fe(II)]}{dt}}{[H_2O_2][Fe(II)]}$ as a

268 function of the fraction of Fe(II)-Glu can be fitted with a linear equation y = ax + b, where a is

269 equal to $1.54 \pm 0.13 \times 10^4$ M^{-1} s^{-1} and represents the rate constant of reaction of Fe(II)-Glu with

270 H_2O_2, and b is equal to rate constant of Fe(II) with H_2O_2 ($-\frac{d[Fe(II)]}{dt}$ data is provided in **Table.**

271 **SM4**). Notably, obtained rate constant is much higher than the rate constant of the classic

272 Fenton reaction which has a rate constant of about 50-70 M^{-1} s^{-1} (Kremer, 2003; Neyens and

273 Baeyens, 2003; Rachmilovich-Calis et al., 2009). Moreover, the value is about five times higher

274 than our recently reported value for the reaction between Fe(II)-oxalate and H_2O_2 (3.2 $\pm$ 0.3

275 $\times 10^3$ M^{-1} s^{-1}) (Scheres Firak et al., 2025). Despite the quantitative difference, both two obtained

276 values are of the same order, highlighting the significant reactivity enhancement conferred by

277 organic ligand coordination. The reason behind this increase is likely due to the Fe(II)-Glu

278 complex accessing a lower reduction potential calculated to be + 0.241 V compared with the

279 Fe(II) (+ 0.771 V) (Strathmann and Stone, 2002), which contributes to the higher rate constant

280 of the reaction of Fe(II)-Glu with H_2O_2.

281 Then the Fenton reaction model was used to fit the experimental data to verify the rate constant

282 value of the reaction between Fe(II)-Glu and H_2O_2. As shown in **Fig. 1a**, the experimental data

283 of Fe(II) kinetics can be well-fitted by the model. The fitted rate constant value of the reaction

284 between Fe(II)-Glu and H_2O_2 was obtained at a range of 1.2×10^4 to 1.8×10^4 M^{-1} s^{-1}, which is

285 very close to the experimental results.
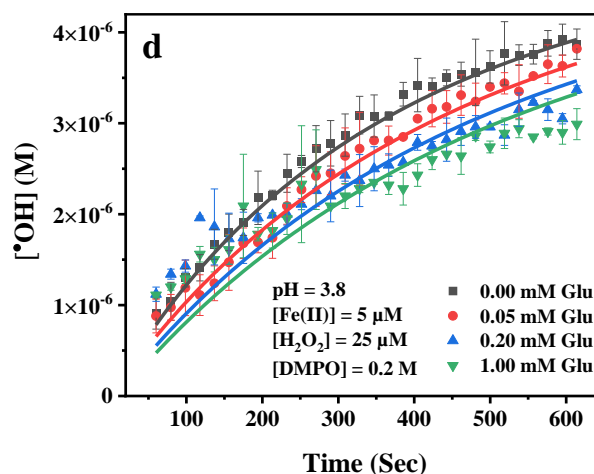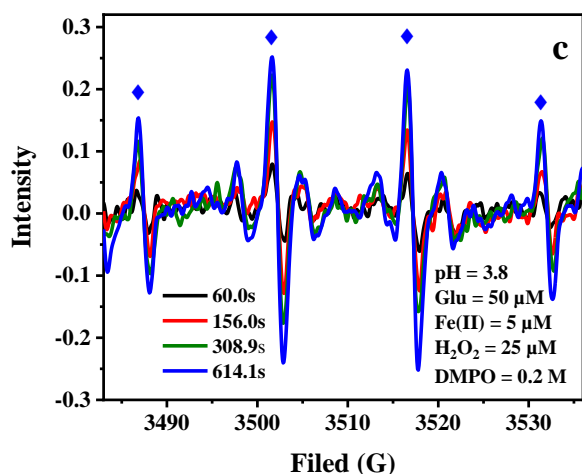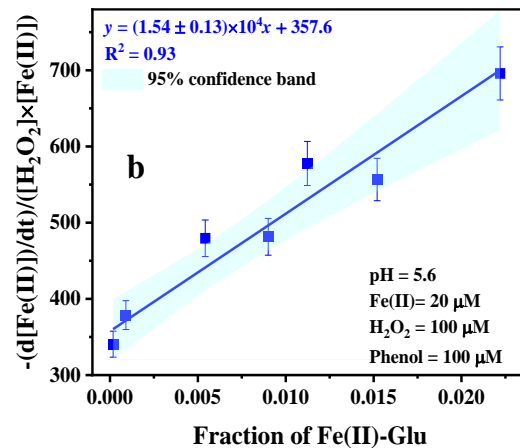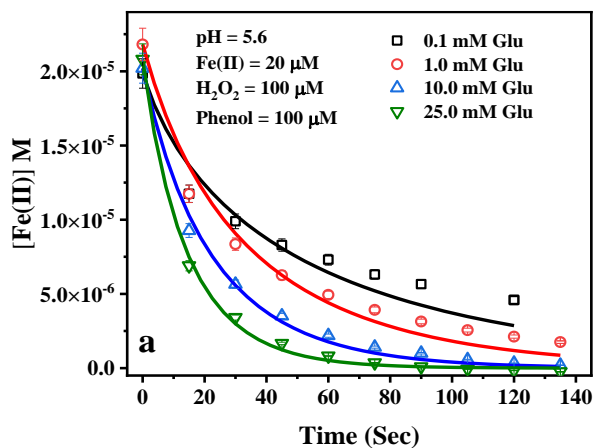
Fig. 1 *Effect of different concentrations of Glu on the kinetics of Fenton reaction (a), apparent rate constant as a function of the fraction of Fe(II)-Glu (b), Signal of EPR corresponding to DMPO-OH (The symbol "◆" marks the position of the characteristic 1:2:2:1 EPR signal of the DMPO-OH adduct.) (c), the kinetics of •OH generation in Fenton reaction in the presence of different concentrations of Glu, (d). Points are determined experimentally, and lines in figures **a** and **d** are the fit of data using the kinetic model.*

3.2.2. •OH quantification

To study the effect of Glu on the •OH generation, EPR experiments were carried out. **Fig. 1c** shows the EPR signal of DMPO-OH (1:2:2:1) increases with the reaction time, indicating that

297 •OH is continuously generated. In **Fig. 1d**, the concentration of generated •OH decreases when

298 the Glu concentration increases from 0 to 1.0 mM. This trend suggests no direct •OH generation

299 occurs from the reaction of Fe(II)-Glu with H_2O_2. This hypothesis has been verified by

300 employing a kinetic model. The experimental data can be well fitted using the experimental rate

301 constant $k_{Fe(II)-Glu/H_2O_2} = 1.54 \pm 0.13 \times 10^4$ M^{-1} s^{-1}.

302 **3.3. Fe(III) photolysis in the presence of Glu**

303 **3.3.1. Fe(II) formation**

304 To study the effect of Glu on the kinetics and determine the quantum yield of the photolysis of

305 Fe(III), the photo-driven reaction was carried out in the presence of different concentrations of

306 Glu (0-200 μM) under simulated solar light. **Fig. SM5a** shows that the Fe(II) generation rate

307 decreases when the Glu concentration increases, which indicates that Glu slightly reduces the

308 photoactivity of Fe(III). As shown in **Fig. 2a**, plotting the apparent quantum yield of Fe(II),

309 $\Phi_{Fe(II)}^{obs}$, as a function of the fraction of Fe(III)-Glu complex, the quantum yield of Fe(II)

310 decreases with the fraction of Fe(III)-Glu complex increasing. The linear fit can depict the

311 kinetic data well with a regression coefficient equal to 0.99. As mentioned in **SM2**, the intercept

312 represents the Fe(II) quantum yield of Fe(III) photolysis under polychromatic irradiation, which

313 is equal to 0.216 ± 0.004. This result is consistent with previous data (Bossmann et al., 1998).

314 The slope represents the difference between Fe(II) quantum yield of the Fe(III) photolysis and

315 the value of the photolysis of Fe(III)-Glu complex ($\Phi_{Fe(III)-Glu}^{Fe(II)} - \Phi_{Fe(III)}^{Fe(II)}$), which is equal to -

316 0.179, hence the Fe(II) quantum yield during the photolysis of Fe(III)-Glu is calculated to be

317 0.037 ± 0.004. Weller et al.(Weller et al., 2013) investigated the photolysis of Fe(III)-

318 carboxylate complexes and found the quantum yield of Fe(II) formation from Fe(III)-malonate

at 308 nm and 351 nm, with values of 0.024 ± 0.001 and 0.040 ± 0.003 respectively. This suggests that Fe(III) complexes containing unsubstituted carboxylates as a functional group exhibit lower quantum yields compared to Fe(III).
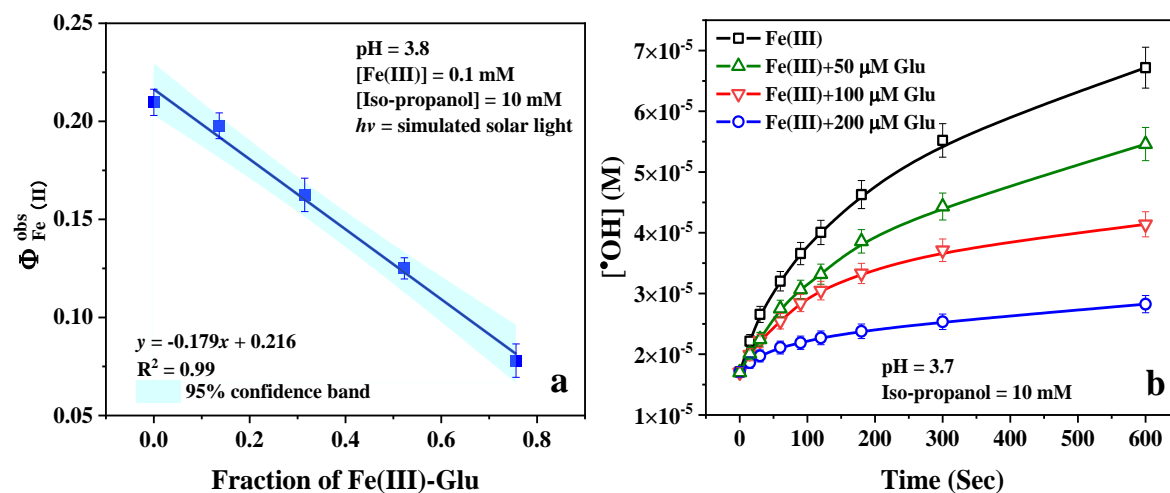

Fig. 2 *a) The quantum yield of Fe(III) photolysis as a function of the fraction of Fe(III)-Glu complex; b) The $^\bullet$OH generation of Fe(III) photolysis in the presence of different concentrations of Glu. The continuous lines are visual guides generated by applying the "Connect B-Spline" function in Origin 2019.*

3.3.2. $^\bullet$OH generation

Since the photolysis of Fe(III) is an important process affecting the budget of $^\bullet$OH in the atmosphere (Guo et al., 2014), the effect of Glu on the $^\bullet$OH produced by the photolysis process of Fe(III) was investigated. As shown in **Fig. SM5b,** the acetone generation rate decreases when the Glu concentration increases, indicating that the $^\bullet$OH generation of the Fe(III) photolysis decreases in the presence of Glu (**Fig. 2b**). The most likely reason for this observation is the decrease of the Fe(III) hydroxy complexes (**Table SM5**), hence the decrease of the $^\bullet$OH yield as the Fe(III)-Glu does not produce $^\bullet$OH directly, but instead forms Glu oxidation products

335 (Glu$_{ox}$) through the LMCT process. These Glu oxidation products can complex Fe(II) and

336 regenerate Fe(III), a mechanism known as "the quenching mechanism" proposed by Wang et

337 al (2010)(Wang et al., 2010). This process reduces the apparent quantum yield of Fe(II) to 0.037

338 ± 0.004. This result illustrates that $^{\bullet}$OH generation could be less in the presence of amino acids

339 during the daytime in the atmosphere.

3.4. The Glu fate in the presence of Fe(III) under simulated solar light

3.4.1 Photodegradation of Glutamic acid in different systems

342 All the above results indicate that Glu not only stabilizes Fe(III)/Fe(II) at higher pH but also

343 influences the Fenton reaction and photolysis of Fe(III) processes. The main effects were that

344 the complexes altered the individual reaction rate constants and $^{\bullet}$OH production. On the other

345 hand, Glu as the organic ligand can also be degraded during the reaction, especially photo-

346 reaction in the atmosphere. **Fig. 3** shows the photodegradation kinetics of Glu in different

347 systems, and the first-order fitted data is reported in **Fig. SM6**. As expected, when only Glu

348 was present in the solution, no significant degradation ($k_{obs} = 1.90 \pm 0.22 \times 10^{-5}$ s^{-1}) was observed

349 after 1 hour of irradiation, as shown in the UV-Vis spectrum (**Fig. SM2**) of Glu, since there is

350 no significant light absorption in the solar spectrum. The Glu degradation slightly increased in

351 the presence of 1 mM H$_2$O$_2$ with a degradation constant of $2.44 \pm 0.45 \times 10^{-5}$ s^{-1} corresponding

352 with a degradation of 8.5 % in 1 hour, which is due to the formation of $^{\bullet}$OH radicals via the

353 photolysis of H$_2$O$_2$. In addition, the rate constant of $^{\bullet}$OH with Glu is 2.3×10^8 M^{-1} s^{-1} (Masuda

354 et al., 1973), which means that the reaction between those two components is one of the most

355 important processes for the degradation of Glu. Considering the second reaction rate constant

356 between $^{\bullet}$OH and H$_2$O$_2$ ($k_{H_2O_2}^{\bullet OH} = 2.7 \times 10^7$ M^{-1} s^{-1}) (Christensen et al., 1982), it can be argued

357 that under adopted conditions, about 55 % of generated •OH was quenched by the H_2O_2, which

358 led to the formation of less reactive hydroperoxyl radical/superoxide anion pair ($HO_2^•/O_2^{•-}$).
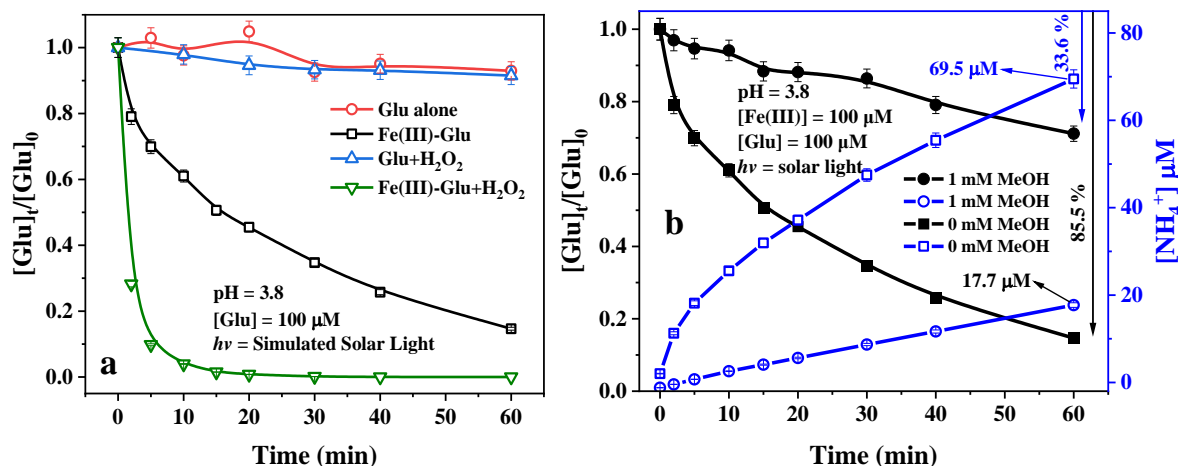
359

360 **Fig. 3** *a) Photodegradation of Glu in different systems: Glu alone, Fe(III)-Glu; Glu+H_2O_2 and*

361 *Fe(III)-Glu+H_2O_2 ([Glu] = 100 μM, [Fe(III)] = 100 μM, [H_2O_2] = 1 mM). b)*

362 *Photodegradation of Glu and ammonium generation in the Fe(III)-Glu system in the absence*

363 *and presence of MeOH. The continuous lines are visual guides generated by applying the*

364 *"Connect B-Spline" function in Origin 2019.*

365 Moreover, in the presence of Fe(III), the mixture of Fe(III)-hydroxy and Fe(III)-Glu complexes

366 underwent the photolysis process. As shown in **Fig. 3a**, about 85 % of Glu was degraded with

367 a first-order rate constant of $4.99 \pm 0.24 \times 10^{-4}$ s^{-1} after 1 hour of irradiation. This high efficiency

368 is likely due to two different Glu degradation pathways, one is due to the reaction between Glu

369 and the •OH radicals generated by photolysis of Fe(III) (R1 and R2), and the other one is due

370 to the direct photolysis of Fe(III)-Glu leading to the formation of Fe(II) and oxidation products

371 of the organic ligand (Glu_{ox}). The synergistic effect of those two processes highly improved the

372 Glu degradation efficiency. To distinguish between the contributions of the two degradation

373 pathways, methanol was selected as •OH scavenger ($k_{Methanol}^{•OH} = 9.7 \times 10^8$ M^{-1} s^{-1}) (Buxton et al.,

374   1988). As illustrated in **Fig. 3b**, Glu degradation was inhibited by 60 %, indicating that 40 %

375   of Glu degradation originates from the photolysis of Fe(III)-Glu complexes. Interestingly, this

376   ratio aligns with the proportion of Fe(III) and Fe(III)-Glu complexes in the system (**Table SM5**),

377   confirming the aforementioned conclusion. Furthermore, the degradation of Glu resulting from

378   the photolysis of Fe(III)-Glu complexes likely does not involve a $^\bullet$OH process (Sun et al., 1998;

379   Weller et al., 2013).

380   Glu degradation was observed to be approximately 100 % after 20 mins of irradiation in the

381   presence of Fe(III) and H_2O_2, with a first-order rate constant of $5.13 \pm 1.03 \times 10^{-3}$ s^{-1}. Compared

382   to conditions with only Fe(III) or H_2O_2, the efficiency of Glu degradation significantly improves

383   due to the photo-Fenton reaction in the system, which greatly accelerates the formation rate of

384   reactive species and consequently enhances the degradation rate of Glu.

385   **3.4.2. Analysis of photodegradation products of glutamic acid**

386   To distinguish the Glu degradation processes resulting from the photolysis of Fe(III)-Glu

387   complexes and from those caused by $^\bullet$OH attack, which might lead to the formation of different

388   products, a series of experiments were conducted. In all cases, IC-MS was employed to analyze

389   the formation of short-chain carboxylic acid and ammonium ions, providing a deeper

390   understanding of the photochemical reaction products in various systems under simulated solar

391   light.

392   **Figure 4a** depicts the formation of ammonium (NH_4^+) in different systems under irradiation. A

393   positive correlation is observed between the rate of NH_4^+ production and the rate of Glu

394   degradation in various systems, suggesting the occurrence of deamination during the Glu

395   degradation. Additionally, several carboxylic acids (i.e. acetic, formic, succinic, malonic, and

396   oxalic acids) were detected (**Table SM6**), as illustrated in **Fig. 4b**, **4c**, and **4d**. Notably, the

397   concentration of generated carboxyl acids is considerably lower than that of NH_4^+.

398   After 120 min of irradiation, low concentrations of generated NH_4^+ and carboxylic acid were

399   determined during Glu photolysis due to small Glu degradation (see **Fig. 4a** and **Fig. SM7**). In

400   the presence of 1 mM H_2O_2, NH_4^+ concentration increased to 7.8 µM within 120 min,

401   representing a 3-fold increase compared to that produced during Glu photolysis. **Fig. 4b**

402   demonstrates the formation of carboxylic acids with formate and succinate as primary

403   carboxylate products, while a negligible concentration of acetate (less than 1 µM) was also

404   detected, all of which are products of $^\bullet OH$ attack.

405   In the presence of Fe(III), NH_4^+ concentration increased to 69.5 µM (**Fig. 4a**) within 60 min.

406   Simultaneously, the generation of carboxyl acids, such as formate, acetate, and oxalate was

407   observed. The concentration of formate initially increased, reaching a maximum value of 8.7

408   µM at 20 min, followed by a decline to about 6.4 µM at 60 min. The reason for the decline is

409   probably due to the reaction of formate with photo-generated $^\bullet OH$ ($k_{Formate}^{^\bullet OH} = 1.3{-}1.4 \times 10^8$ M$^-$

410   ^{1} s^{-1}) (Buxton et al., 1988). Acetate concentration steadily increased throughout the reaction,

411   reaching 10.9 µM at 60 min. Other carboxylates, such as succinate, malonate, and oxalate, were

412   found in lower concentration, with a maximum of around 2 µM within 5 min. As mentioned

413   above, in the presence of Fe(III), the Glu degradation can be attributed to two pathways: one

414   resulting from $^\bullet OH$ attack, on the other from the photolysis of the Fe(III)-Glu complexes.

415

416
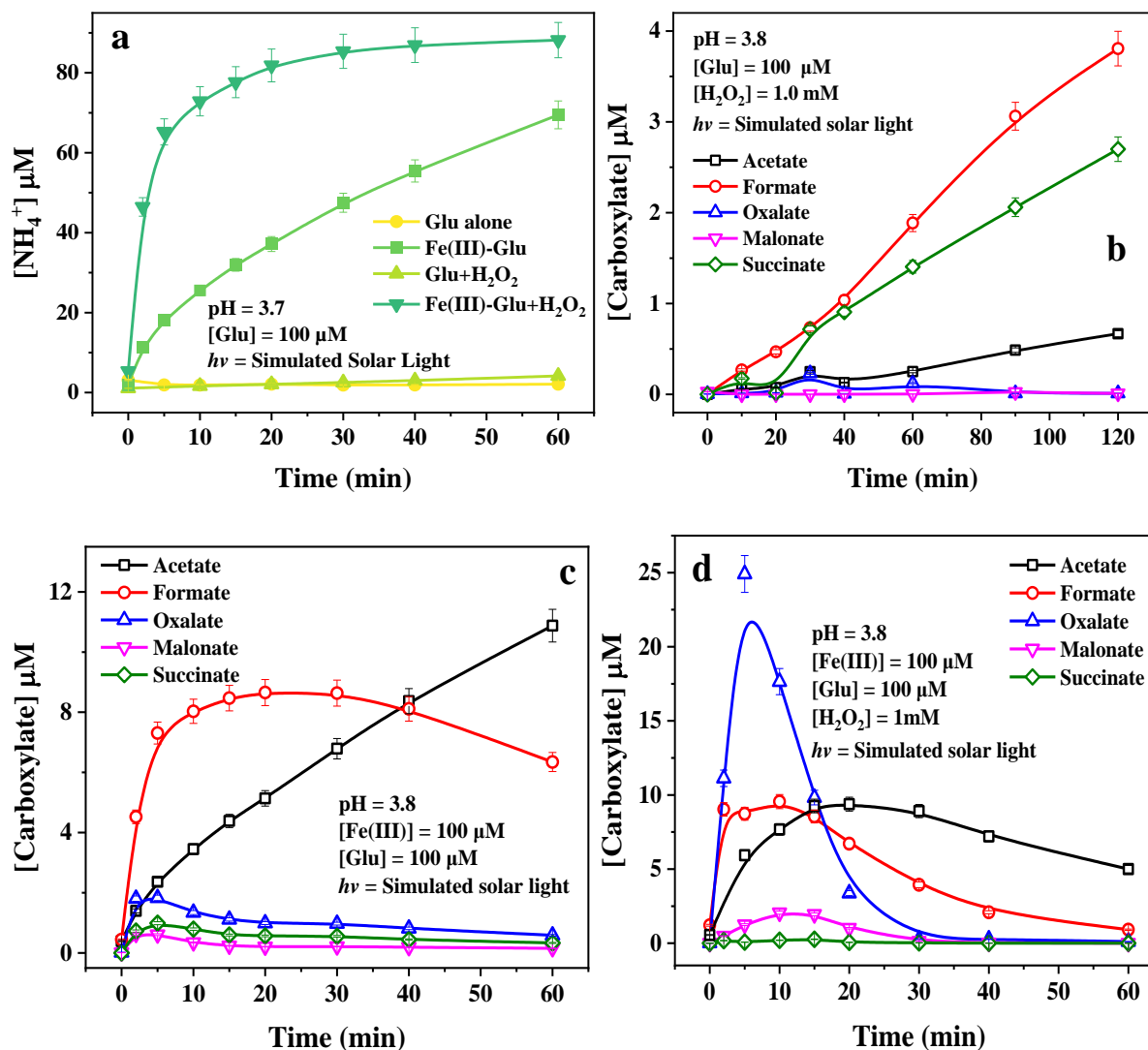
Fig. 4. *The by-products of Glu degradation under solar light a) formation of NH₄⁺ in different systems; formation of carboxylic acids b) in the system Glu+H₂O₂; c) in the system Glu+Fe(III) and d) in the system Glu+Fe(III)+H₂O₂. The continuous lines are visual guides generated by applying the "Connect B-Spline" function in Origin 2019.*

To distinguish the contribution of these two pathways, isopropanol was employed to quench $^{\bullet}OH$ in solution generating acetone as the main product (Motohashi and Saito, 1993). As shown in **Fig. SM8**, only acetate and formate were generated (succinate, malonate, and oxalate were not detected). Moreover, the presence of isopropanol significantly enhanced the formation of

425   acetate compared to values observed with only Fe(III) and Glu. This is likely due to the H-

426   donor effect of the added alcohol or to the reaction between acetic acid radicals (HOOCCH$_2{}^\bullet$)

427   and HO$_2{}^\bullet$ radicals, the latter being generated through the reaction of $^\bullet$OH with the alcohol. As

428   shown in **Fig. SM8**, the concentration of generated formate in the presence of isopropanol and

429   Fe(III) is lower than that when only Fe(III) is added, suggesting that formate was likely not a

430   primary product generated from the photolysis of Fe(III)-Glu complexes but rather may be

431   produced by $^\bullet$OH attack of other carboxylic acids. For example, the generated acetate can be

432   further oxidized reacting with $^\bullet$OH leading to the formation of formate.

433   This finding is consistent with the result observed in the presence of H$_2$O$_2$ alone (**Fig. SM7**). In

434   the presence of $^\bullet$OH scavenger, the generation of NH$_4{}^+$ was strongly inhibited with the

435   formation of 17.7 µM instead of 69.5 µM after 1 h (as previously reported in **Fig. 3b**), which

436   indicates that the NH$_4{}^+$ formation is mainly due to the $^\bullet$OH attack process. Furthermore, a

437   significant NH$_4{}^+$ (up to 69.5 µM within 60 min) can be observed in the presence of both Fe(III)

438   and H$_2$O$_2$ (**Fig.4d**). Oxalate, acetate, and formate were observed as the predominant carboxylate

439   products with higher concentrations, reaching 24.9, 9.4, and 9.6 µM respectively, before

440   decreasing. Additionally, the formations of malonate (2.1 µM) and succinate (0.3 µM) were

441   observed at lower concentrations during the photoreaction. In the presence of H$_2$O$_2$ and Fe(III),

442   the Fe(III)/Fe(II)-cycle is enhanced via the photo-Fenton reaction. Fe(II) is rapidly re-oxidized

443   to Fe(III) to produce $^\bullet$OH, which then directly attacks Glu, leading to degradation. Fe(III) is re-

444   complexed by Glu reactivating the photoreaction and then the iron cycle. Therefore, the

445   addition of H$_2$O$_2$ favors deamination as well as various carbon-centered radical combination

446   interactions. The rapid depletion of oxalate after 30 min implies that photolysis of complexes

447   between Fe(III) and polycarboxylic acid also occurs in this system, while formate, acetate, and

448   malonate exhibit similar tendencies with different reaction rates. To verify the mineralization

449   of Glu during the reaction, a TOC was followed during the reaction. As shown in **Fig. SM9a**,

450   the mineralization efficiency of Glu in the presence of Fe(III) and H_2O_2 is significantly higher

451   than that observed when only Fe(III) is present, due to the presence of the photo-Fenton process.

452   This finding is consistent with the degradation efficiency of Glu presented in **Figure 3a**. Hence,

453   these results illustrate that Glu was mineralized to form CO_2 and H_2O. Moreover, the TOC

454   values obtained experimentally are higher than the values calculated from the concentration of

455   Glu and carboxylic acid products, indicating the presence of other organic compounds in the

456   system. Along these organic substances cannot be detected under our experimental conditions,

457   they will enter the cloud water gas phase, further participating in atmospheric photochemical

458   reactions and eventually being mineralized into H_2O and CO_2. In the presence of H_2O_2, as Glu

459   undergoes photodegradation, the concentration of H_2O_2 in the system continues to decrease

460   until it is completely consumed (**Fig. SM9b**).

461   **3.5. Insight into the mechanism of Glu transformation**

462   The light-driven transformation mechanism of Glu in the presence of Fe(III) was investigated,

463   with a focus on the $^{\bullet}OH$-mediated and the ligand-to-metal charge transfer (LMCT) process. The

464   key difference between the two processes lies in the generation of glutamate radials: the $^{\bullet}OH$-

465   mediated process involves a free radical mechanism initiated by hydrogen abstraction, whereas

466   the LMCT pathway proceeds via an electron transfer process driven by photoexcitation. To

467   provide a clear comparison, the two mechanisms are illustrated separately in **Scheme. 1**

468   summarizing the possible Glu degradation pathway, derived from IC-MS analysis of the

469   detected products.

470   In the $^\bullet$OH-mediated process, the α- carbon of Glu is identified as the primary site attacked for

471    $^\bullet$OH attack, initiating the transformation process. Hydrogen abstraction by $^\bullet$OH results in the

472   formation of glutamate alkyl radical (R-C$^\bullet$(COO$^-$)NH$_3^+$) and H$_2$O. Subsequently, this alkyl

473   radical reacts with O$_2$ to generate the alkylperoxy radical (ROO$^\bullet$), which is further converted to

474   alkoxy radical (RO$^\bullet$) (Goldman et al., 2021; von Sonntag and Schuchmann, 1991). The

475   formation of RO$^\bullet$ is followed by a deamination process, which leads to the formation of

476   ammonium (NH$_4^+$) and 2-oxoadipic acid through the cleavage of the amino group (Vel Leitner

477   et al., 2002). Due to the presence of an oxo group (C=O) adjacent to a carboxyl group (COOH),

478   2-oxoadipic acid is chemically unstable and prone to self-decomposition via decarboxylation,

479   resulting in the formation of succinic acid (Penteado et al., 2019). Further oxidation of succinic

480   acid produces smaller carboxylic acids (Charbouillot et al., 2012).

481   In contrast, the LMCT process is initiated upon irradiation, resulting in the reduction of Fe(III)

482   to Fe(II) and the generation of a radical centered on the oxygen atom of α-carboxyl group of

483   glutamic acid (R-CH(NH$_3^+$)C$^+$O$^\bullet$O$^-$). This high reactive radical undergoes a decarboxylation

484   process resulting in the formation of an alkyl radical (R-CH$^\bullet$NH$_3^+$). Subsequently, the radical

485   chain reaction propagates in the presence of O$_2$, leading to the formation of smaller carboxylic

486   acids. It is critical to highlight that the only carboxylic acids detected under the same conditions

487   are formic acid and acetic acid. This is different from the $^\bullet$OH-mediated process, in which

488   succinate is first formed and then further decomposed into compounds such as other small

489   molecular carboxylic acids.

490

491
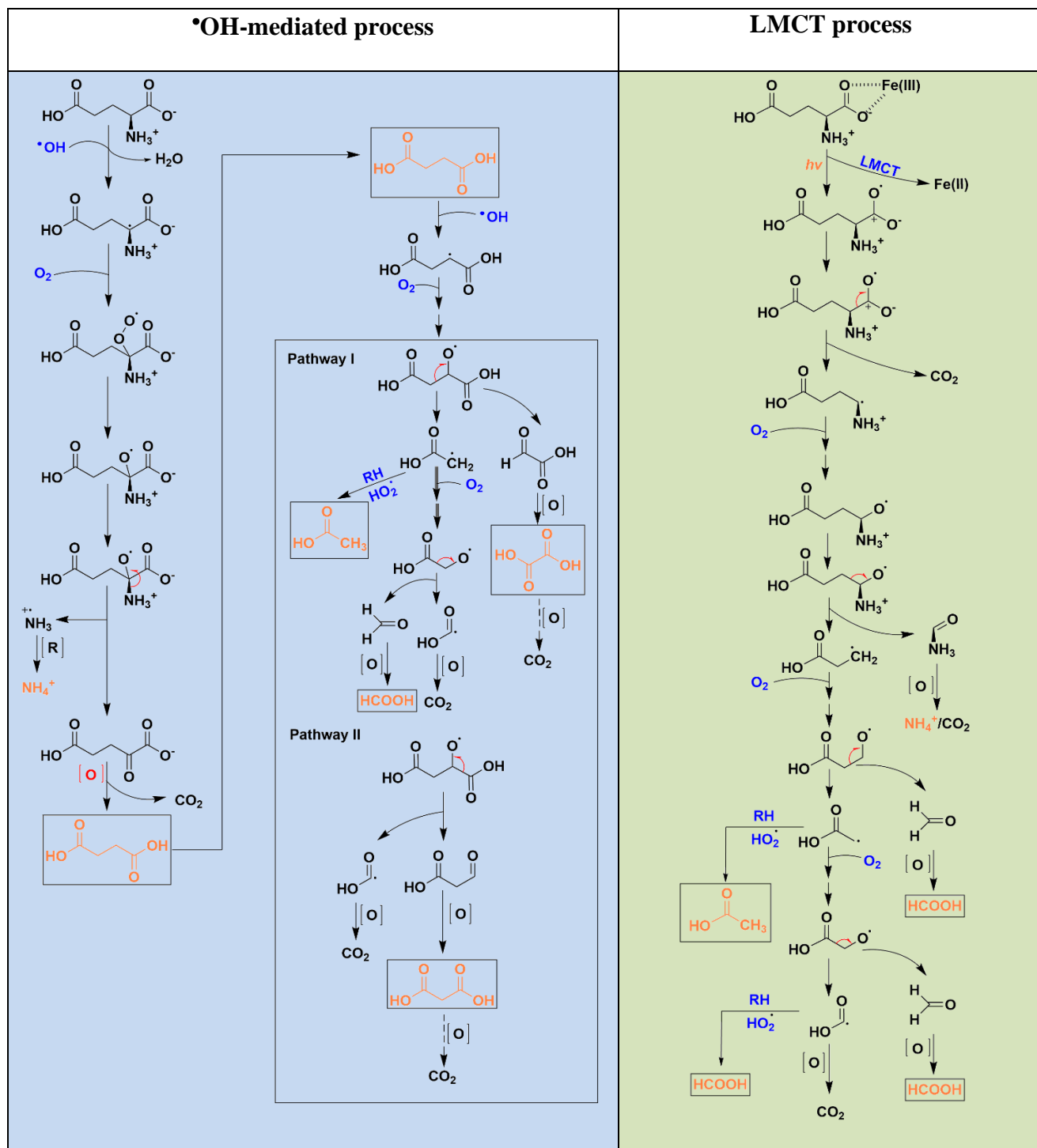
492   **Scheme 1.** *The mechanism of Glu degradation in the presence of Fe(III): by •OH attacking*

493   *process and LMCT process. Products in orange are detected by IC-MS.*

494

4. ATMOSPHERIC IMPLICATION

This study systematically investigated the complexation of Glu with Fe(II)/Fe(III), its effect on the typical atmospheric reactions (Fenton reaction and Fe(III) photolysis), and its fate in the atmospheric aqueous phase. Our findings reveal that iron-amino acid complexes (Fe-AAs) significantly modify the Fe(II)/Fe(III) cycle and $^\bullet$OH budget, diverging from the "classic" photo-Fenton mechanisms. Specifically, Fe(II)-Glu reacts with H_2O_2 at a rate constant two orders of magnitude higher than Fe(II) alone, potentially improving the iron cycle. Conversely, Fe(III)-Glu exhibits a lower quantum yield under irradiation, suppressing the Fe(III)/Fe(II) cycle. Moreover, both reactions result in lower $^\bullet$OH generation, as they favor the formation of Glu oxidation products (Glu_{ox}), thus partially affecting atmospheric oxidative capacity.

To date, the concentration of the Fe(II)/Fe(III)-Glu in cloud water has not yet been directly measured. Hence, based on the reported mean concentrations of Glu (87 nM) (Renard et al., 2022), Fe(II) (1 µM) (Deguillaume et al., 2014), and Fe(III) (0.5 µM) (Deguillaume et al., 2014) in cloud water from the Puy de Dôme station (PUY - France), the fraction of Fe(II)-Glu and Fe(III)-Glu was calculated to be around 8.7×10^{-10} - 2.1×10^{-4} % and 6.1×10^{-2} - 2.4×10^{-1} % using Hyss software at a pH range of 3 - 7, respectively. Cloud water span a wide pH range (3–7), which influences iron speciation and redox cycling. Low pH enhances iron solubility but may reduce Fe–Glu complexation by altering ligand binding. Nevertheless, in polluted regions with elevated iron and amino acid levels, the absolute Fe–Glu concentration may remain appreciable despite a lower complexation fraction. In contrast, marine clouds often contain lower concentrations of both Fe and amino acid (like Glu is around 33 pM collected in Venice on the Sacca San Biagio Island (Barbaro et al., 2011)), leading to a smaller Fe-Glu fraction. Moreover, the concentration of Glu in cloud droplets may increase during the cloud water evaporation,

518 leading to an increase in the concentration of iron-Glu complexes. This shift could alter

519 atmospheric Fenton reaction dynamics, reducing $^{\bullet}$OH production, particularly at night

520 (Galloway et al., 2014; Shulman et al., 1997). Similarly, the lower quantum yield of the Fe(III)-

521 Glu under irradiation inhibits the Fe(II)/Fe(III) cycle and $^{\bullet}$OH generation especially in daytime

522 conditions. Likewise, the variations in light intensity due to diurnal cycles and cloud cover

523 modulate the photolysis rates of iron–ligand complexes and the generation of reactive radicals.

524 Taken together, these factors suggest that the photochemical processes involving Fe–Glu

525 complexes are highly condition-dependent, leading to variable degradation and pathways of

526 amino acids in atmospheric aqueous phases. This underscores the need to incorporate such

527 environmental dependencies into atmospheric models.

528 In addition, recent studies reported that the average AAs contribution corresponded to 9.1 % of

529 the dissolved organic carbon (DOC) (Bianco et al., 2016), highlighting their significance. Hence,

530 Fe-AAs play a crucial role in iron speciation, stability, and $^{\bullet}$OH budget in atmospheric aqueous

531 phases, which suggests that the inclusion of Fe-AAs in atmospheric aqueous phase models is

532 essential for accurately estimating $^{\bullet}$OH production, a key driver of atmospheric oxidation.

533 Moreover, irradiation of Glu in the presence of Fe(III), demonstrated two different mechanisms

534 ($^{\bullet}$OH mediated and LMCT process) leading to the generation of different products, which can

535 further influence the atmospheric chemical composition, particularly through the formation of

536 aqueous secondary organic aerosols (aqSOA) (Ervens et al., 2014). Overall, the observed

537 generation of NH_4^+ during the Glu photo-degradation suggests a potential transformation

538 pathway from organic nitrogen to inorganic nitrogen species in cloud water, providing a

539 mechanistic link between organic nitrogen and ammonium. This finding is in line with previous

540 reports (Mopper and Zika, 1987) that emphasize the role of amino acids in nitrogen cycling in

541 the atmosphere. The generation of carboxylic acids further increases atmospheric complexity,

542 as the generated carboxylic acids (e.g., oxalic acid) can complex iron and influence consequent

543 photochemistry. In fact, atmospheric models often simplify the distribution and interactions of

544 transition metal ions (TMIs) with organic compounds, including AAs. This study highlights the

545 crucial role of the LMCT process in AAs oxidation, which should be considered in atmospheric

546 modeling as well.

547 **ACKNOWLEDGMENT**

550 **AUTHOR CONTRIBUTION**

551 **PC:** Investigation, Formal analysis, Writing – original draft**; GM:** Funding acquisition, Review

552 & editing, Supervision**; MS:** Review & editing, Supervision**, GV:** Technical support**; DSF, TS,**

553 **HH:** Review & editing**; MB:** Conceptualization, Writing-review & editing, Supervision.

554 **REFERENCE**

555 Alpert, P. A., Dou, J., Corral Arroyo, P., Schneider, F., Xto, J., Luo, B., Peter, T., Huthwelker,

556 T., Borca, C. N., Henzler, K. D., Schaefer, T., Herrmann, H., Raabe, J., Watts, B., Krieger, U.

557 K., and Ammann, M.: Photolytic radical persistence due to anoxia in viscous aerosol particles,

558 Nature Communications, 12, 1769, https://doi.org/10.1038/s41467-021-21913-x, 2021.

559 Angle, K. J., Neal, E. E., and Grassian, V. H.: Enhanced Rates of Transition-Metal-Ion-

560 Catalyzed Oxidation of S(IV) in Aqueous Aerosols: Insights into Sulfate Aerosol Formation in

561 the Atmosphere, Environmental Science & Technology, 55, 10291–10299,

562 https://doi.org/10.1021/acs.est.1c01932, 2021.

563   Bader, H., Sturzenegger, V., and Hoigné, J.: Photometric method for the determination of low

564   concentrations of hydrogen peroxide by the peroxidase catalyzed oxidation of N,N-diethyl-*p*-

565   phenylenediamine (DPD), Water Research, 22, 1109–1115, https://doi.org/10.1016/0043-

566   1354(88)90005-X, 1988.

567   Barbaro, E., Zangrando, R., Moret, I., Barbante, C., Cescon, P., and Gambaro, A.: Free amino

568   acids in atmospheric particulate matter of Venice, Italy, Atmospheric Environment, 45, 5050–

569   5057, https://doi.org/10.1016/j.atmosenv.2011.01.068, 2011.

570   Battaglia Jr., M. A., Weber, R. J., Nenes, A., and Hennigan, C. J.: Effects of water-soluble

571   organic carbon on aerosol pH, Atmospheric Chemistry and Physics, 19, 14607–14620,

572   https://doi.org/10.5194/acp-19-14607-2019, 2019.

573   Bianco, A., Passananti, M., Perroux, H., Voyard, G., Mouchel-Vallon, C., Chaumerliac, N.,

574   Mailhot, G., Deguillaume, L., and Brigante, M.: A better understanding of hydroxyl radical

575   photochemical sources in cloud waters collected at the puy de Dôme station – experimental

576   versus modelled formation rates, Atmospheric Chemistry and Physics, 15, 9191–9202,

577   https://doi.org/10.5194/acp-15-9191-2015, 2015.

578   Bianco, A., Voyard, G., Deguillaume, L., Mailhot, G., and Brigante, M.: Improving the

579   characterization of dissolved organic carbon in cloud water: Amino acids and their impact on

580   the oxidant capacity, Scientific Reports, 6, 37420, https://doi.org/10.1038/srep37420, 2016.

581   Bianco, A., Vaïtilingom, M., Bridoux, M., Chaumerliac, N., Pichon, J.-M., Piro, J.-L., and

582   Deguillaume, L.: Trace Metals in Cloud Water Sampled at the Puy De Dôme Station,

583   Atmosphere, 8, 225, https://doi.org/10.3390/atmos8110225, 2017.

584   Bianco, A., Deguillaume, L., Vaïtilingom, M., Nicol, E., Baray, J.-L., Chaumerliac, N., and

585   Bridoux, M.: Molecular Characterization of Cloud Water Samples Collected at the Puy de

586 Dôme (France) by Fourier Transform Ion Cyclotron Resonance Mass Spectrometry,

587 Environmental Science & Technology, 52, 10275–10285,

588 https://doi.org/10.1021/acs.est.8b01964, 2018.

589 Bianco, A., Passananti, M., Brigante, M., and Mailhot, G.: Photochemistry of the Cloud

590 Aqueous Phase: A Review, Molecules, 25, 423, https://doi.org/10.3390/molecules25020423,

591 2020.

592 Bossmann, S. H., Oliveros, E., Göb, S., Siegwart, S., Dahlen, E. P., Payawan, L., Straub, M.,

593 Wörner, M., and Braun, A. M.: New Evidence against Hydroxyl Radicals as Reactive

594 Intermediates in the Thermal and Photochemically Enhanced Fenton Reactions, The Journal of

595 Physical Chemistry A, 102, 5542–5550, https://doi.org/10.1021/jp980129j, 1998.

596 Buxton, G. V., Greenstock, C. L., Helman, W. P., and Ross, A. B.: Critical Review of rate

597 constants for reactions of hydrated electrons, hydrogen atoms and hydroxyl radicals ($\cdot$OH/$\cdot$O−

598 in Aqueous Solution, Journal of Physical and Chemical Reference Data, 17, 513–886,

599 https://doi.org/10.1063/1.555805, 1988.

600 Charbouillot, T., Gorini, S., Voyard, G., Parazols, M., Brigante, M., Deguillaume, L., Delort,

601 A.-M., and Mailhot, G.: Mechanism of carboxylic acid photooxidation in atmospheric aqueous

602 phase: Formation, fate and reactivity, Atmospheric Environment, 56, 1–8,

603 https://doi.org/10.1016/j.atmosenv.2012.03.079, 2012.

604 Christensen, H., Sehested, K., and Corfitzen, H.: Reactions of hydroxyl radicals with hydrogen

605 peroxide at ambient and elevated temperatures, The Journal of Physical Chemistry, 86, 1588–

606 1590, https://doi.org/10.1021/j100206a023, 1982.

607 Deguillaume, L., Charbouillot, T., Joly, M., Vaïtilingom, M., Parazols, M., Marinoni, A.,

608 Amato, P., Delort, A.-M., Vinatier, V., Flossmann, A., Chaumerliac, N., Pichon, J. M., Houdier,

S., Laj, P., Sellegri, K., Colomb, A., Brigante, M., and Mailhot, G.: Classification of clouds sampled at the puy de Dôme (France) based on 10 yr of monitoring of their physicochemical properties, Atmospheric Chemistry and Physics, 14, 1485–1506, https://doi.org/10.5194/acp-14-1485-2014, 2014.

Edwards, K. C., Klodt, A. L., Galeazzo, T., Schervish, M., Wei, J., Fang, T., Donahue, N. M., Aumont, B., Nizkorodov, S. A., and Shiraiwa, M.: Effects of Nitrogen Oxides on the Production of Reactive Oxygen Species and Environmentally Persistent Free Radicals from α-Pinene and Naphthalene Secondary Organic Aerosols, The Journal of Physical Chemistry A, 126, 7361–7372, https://doi.org/10.1021/acs.jpca.2c05532, 2022.

Ervens, B., Sorooshian, A., Lim, Y. B., and Turpin, B. J.: Key parameters controlling OH-initiated formation of secondary organic aerosol in the aqueous phase (aqSOA), Journal of Geophysical Research: Atmospheres, 119, 3997–4016, https://doi.org/10.1002/2013JD021021, 2014.

Gabet, A., Guy, C., Fazli, A., Métivier, H., de Brauer, C., Brigante, M., and Mailhot, G.: The ability of recycled magnetite nanoparticles to degrade carbamazepine in water through photo-Fenton oxidation at neutral pH, Separation and Purification Technology, 317, 123877, https://doi.org/10.1016/j.seppur.2023.123877, 2023.

Galloway, M. M., Powelson, M. H., Sedehi, N., Wood, S. E., Millage, K. D., Kononenko, J. A., Rynaski, A. D., and De Haan, D. O.: Secondary Organic Aerosol Formation during Evaporation of Droplets Containing Atmospheric Aldehydes, Amines, and Ammonium Sulfate, Environmental Science & Technology, 48, 14417–14425, https://doi.org/10.1021/es5044479, 2014.

Gligorovski, S., Strekowski, R., Barbati, S., and Vione, D.: Environmental Implications of Hydroxyl Radicals ((•)OH), Chemical Reviews, 115, 13051–13092, https://doi.org/10.1021/cr500310b, 2015.

Goldman, M. J., Green, W. H., and Kroll, J. H.: Chemistry of Simple Organic Peroxy Radicals under Atmospheric through Combustion Conditions: Role of Temperature, Pressure, and NOx Level, The Journal of Physical Chemistry A, 125, 10303–10314, https://doi.org/10.1021/acs.jpca.1c07203, 2021.

Guo, J., Tilgner, A., Yeung, C., Wang, Z., Louie, P. K. K., Luk, C. W. Y., Xu, Z., Yuan, C., Gao, Y., Poon, S., Herrmann, H., Lee, S., Lam, K. S., and Wang, T.: Atmospheric Peroxides in a Polluted Subtropical Environment: Seasonal Variation, Sources and Sinks, and Importance of Heterogeneous Processes, Environmental Science & Technology, 48, 1443–1450, https://doi.org/10.1021/es403229x, 2014.

Hoops, S., Sahle, S., Gauges, R., Lee, C., Pahle, J., Simus, N., Singhal, M., Xu, L., Mendes, P., and Kummer, U.: COPASI—a COmplex PAthway SImulator, Bioinformatics, 22, 3067–3074, https://doi.org/10.1093/bioinformatics/btl485, 2006.

Kanakidou, M., Myriokefalitakis, S., and Tsigaridis, K.: Aerosols in atmospheric chemistry and biogeochemical cycles of nutrients, Environmental Research Letters, 13, 063004, https://doi.org/10.1088/1748-9326/aabcdb, 2018.

Kremer, M. L.: The Fenton Reaction. Dependence of the Rate on pH, The Journal of Physical Chemistry A, 107, 1734–1741, https://doi.org/10.1021/jp020654p, 2003.

Long, Y., Charbouillot, T., Brigante, M., Mailhot, G., Delort, A.-M., Chaumerliac, N., and Deguillaume, L.: Evaluation of modeled cloud chemistry mechanism against laboratory

653 irradiation experiments: The HxOy/iron/carboxylic acid chemical system, Atmospheric

654 Environment, 77, 686–695, https://doi.org/10.1016/j.atmosenv.2013.05.037, 2013.

655 Mace, K. A., Kubilay, N., and Duce, R. A.: Organic nitrogen in rain and aerosol in the eastern

656 Mediterranean atmosphere: An association with atmospheric dust, Journal of Geophysical

657 Research: Atmospheres, 108, https://doi.org/10.1029/2002JD002997, 2003.

658 Marion, A., Brigante, M., and Mailhot, G.: A new source of ammonia and carboxylic acids in

659 cloud water: The first evidence of photochemical process involving an iron-amino acid complex,

660 Atmospheric Environment, 195, 179–186, https://doi.org/10.1016/j.atmosenv.2018.09.060,

661 2018.

662 Masuda, T., Nakano, S., and Kondo, M.: Rate constants for the reactions of OH radicals with

663 the enzyme proteins as determined by the p-nitrosodimethylaniline method, Journal of

664 Radiation Research, 14, 339–345, https://doi.org/10.1269/jrr.14.339, 1973.

665 Matos, J. T. V., Duarte, R. M. B. O., and Duarte, A. C.: Challenges in the identification and

666 characterization of free amino acids and proteinaceous compounds in atmospheric aerosols: A

667 critical review, TrAC Trends in Analytical Chemistry, 75, 97–107,

668 https://doi.org/10.1016/j.trac.2015.08.004, 2016.

669 Mopper, K. and Zika, R. G.: Free amino acids in marine rains: evidence for oxidation and

670 potential role in nitrogen cycling, Nature, 325, 246–249, https://doi.org/10.1038/325246a0,

671 1987.

672 Motohashi, N. and Saito, Y.: Competitive Measurement of Rate Constants for Hydroxyl Radical

673 Reactions Using Radiolytic Hydroxylation of Benzoate, Chemical & Pharmaceutical Bulletin,

674 41, 1842–1845, https://doi.org/10.1248/cpb.41.1842, 1993.

Neyens, E. and Baeyens, J.: A review of classic Fenton's peroxidation as an advanced oxidation technique, Journal of Hazardous Materials, 98, 33–50, https://doi.org/10.1016/S0304-3894(02)00282-0, 2003.

Penteado, F., Lopes, E. F., Alves, D., Perin, G., Jacob, R. G., and Lenardão, E. J.: α-Keto Acids: Acylating Agents in Organic Synthesis, Chemical Reviews, 119, 7113–7278, https://doi.org/10.1021/acs.chemrev.8b00782, 2019.

van Pinxteren, M., Müller, C., Iinuma, Y., Stolle, C., and Herrmann, H.: Chemical Characterization of Dissolved Organic Compounds from Coastal Sea Surface Microlayers (Baltic Sea, Germany), Environmental Science & Technology, 46, 10455–10462, https://doi.org/10.1021/es204492b, 2012.

van Pinxteren, M., Zeppenfeld, S., Fomba, K. W., Triesch, N., Frka, S., and Herrmann, H.: Amino acids, carbohydrates, and lipids in the tropical oligotrophic Atlantic Ocean: sea-to-air transfer and atmospheric in situ formation, Atmospheric Chemistry and Physics, 23, 6571–6590, https://doi.org/10.5194/acp-23-6571-2023, 2023.

Pye, H. O. T., Nenes, A., Alexander, B., Ault, A. P., Barth, M. C., Clegg, S. L., Collett, J. L., Fahey, K. M., Hennigan, C. J., Herrmann, H., Kanakidou, M., Kelly, J. T., Ku, I.-T., McNeill, V. F., Riemer, N., Schaefer, T., Shi, G., Tilgner, A., Walker, J. T., Wang, T., Weber, R., Xing, J., Zaveri, R. A., and Zuend, A.: The Acidity of Atmospheric Particles and Clouds, Atmos Chem Phys, 20, 4809–4888, https://doi.org/10.5194/acp-20-4809-2020, 2020.

Rachmilovich-Calis, S., Masarwa, A., Meyerstein, N., Meyerstein, D., and van Eldik, R.: New Mechanistic Aspects of the Fenton Reaction, Chemistry – A European Journal, 15, 8303–8309, https://doi.org/10.1002/chem.200802572, 2009.

Renard, P., Brissy, M., Rossi, F., Leremboure, M., Jaber, S., Baray, J.-L., Bianco, A., Delort, A.-M., and Deguillaume, L.: Free amino acid quantification in cloud water at the Puy de Dôme station (France), Atmospheric Chemistry and Physics, 22, 2467–2486, https://doi.org/10.5194/acp-22-2467-2022, 2022.

Samavat, S., Gholami, N., and Nazari, K.: Complexation of Iron (III) With Citrate and Tartarate Anions in Perturbed Aqueous Solutions Using Potentiometry and Difference UV/Vis. and IR Spectrophotometric Methods., Acta Chimica Slovenica, 54, 2007.

Samy, S., Robinson, J., and Hays, M. D.: An advanced LC-MS (Q-TOF) technique for the detection of amino acids in atmospheric aerosols, Analytical and Bioanalytical Chemistry, 401, 3103–3113, https://doi.org/10.1007/s00216-011-5238-2, 2011.

Scheres Firak, D., Schaefer, T., Senff, P., Cheng, P., Sarakha, M., Brigante, M., Mailhot, G., and Herrmann, H.: Fenton-like Reactions in Acidic Environments: New Mechanistic Insights and Implications to Atmospheric Particle-Phase Chemistry, ACS E&ST Air, https://doi.org/10.1021/acsestair.5c00077, 2025.

Shah, V., Jacob, D. J., Moch, J. M., Wang, X., and Zhai, S.: Global modeling of cloud water acidity, precipitation acidity, and acid inputs to ecosystems, Atmospheric Chemistry and Physics, 20, 12223–12245, https://doi.org/10.5194/acp-20-12223-2020, 2020.

Shulman, M. L., Charlson, R. J., and James Davis, E.: The effects of atmospheric organics on aqueous droplet evaporation, Journal of Aerosol Science, 28, 737–752, https://doi.org/10.1016/S0021-8502(96)00469-7, 1997.

von Sonntag, C. and Schuchmann, H.-P.: The Elucidation of Peroxyl Radical Reactions in Aqueous Solution with the Help of Radiation-Chemical Methods, Angewandte Chemie International Edition in English, 30, 1229–1253, https://doi.org/10.1002/anie.199112291, 1991.

720 Soriano-Molina, P., García Sánchez, J. L., Alfano, O. M., Conte, L. O., Malato, S., and Sánchez

721 Pérez, J. A.: Mechanistic modeling of solar photo-Fenton process with Fe^{3+}-EDDS at neutral

722 pH, Applied Catalysis B: Environmental, 233, 234–242,

723 https://doi.org/10.1016/j.apcatb.2018.04.005, 2018.

724 Sorooshian, A., Wang, Z., Coggon, M. M., Jonsson, H. H., and Ervens, B.: Observations of

725 Sharp Oxalate Reductions in Stratocumulus Clouds at Variable Altitudes: Organic Acid and

726 Metal Measurements During the 2011 E-PEACE Campaign, Environmental Science &

727 Technology, 47, 7747–7756, https://doi.org/10.1021/es4012383, 2013.

728 Strathmann, T. J. and Stone, A. T.: Reduction of Oxamyl and Related Pesticides by FeII:

729 Influence of Organic Ligands and Natural Organic Matter, Environmental Science &

730 Technology, 36, 5172–5183, https://doi.org/10.1021/es0205939, 2002.

731 Sun, L., Wu, C.-H., and Faust, B. C.: Photochemical Redox Reactions of Inner-Sphere

732 Copper(II)-Dicarboxylate Complexes: Effects of the Dicarboxylate Ligand Structure on

733 Copper(I) Quantum Yields, The Journal of Physical Chemistry A, 102, 8664–8672,

734 https://doi.org/10.1021/jp982045g, 1998.

735 Tilgner, A., Bräuer, P., Wolke, R., and Herrmann, H.: Modelling multiphase chemistry in

736 deliquescent aerosols and clouds using CAPRAM3.0i, Journal of Atmospheric Chemistry, 70,

737 221–256, https://doi.org/10.1007/s10874-013-9267-4, 2013.

738 Triesch, N., van Pinxteren, M., Salter, M., Stolle, C., Pereira, R., Zieger, P., and Herrmann, H.:

739 Sea Spray Aerosol Chamber Study on Selective Transfer and Enrichment of Free and Combined

740 Amino Acids, ACS Earth and Space Chemistry, 5, 1564–1574,

741 https://doi.org/10.1021/acsearthspacechem.1c00080, 2021.

742 Vel Leitner, N. K., Berger, P., and Legube, B.: Oxidation of Amino Groups by Hydroxyl

743 Radicals in Relation to the Oxidation Degree of the α-Carbon, Environmental Science &

744 Technology, 36, 3083–3089, https://doi.org/10.1021/es0101173, 2002.

745 Wang, T. L., Tong, H. W., Yan, X. Y., Sheng, L. Q., Yang, J., and Liu, S. M.: Determination

746 of Volatile Carbonyl Compounds in Cigarette Smoke by LC-DAD, Chromatographia, 62, 631–

747 636, https://doi.org/10.1365/s10337-005-0675-8, 2005.

748 Wang, Z., Chen, X., Ji, H., Ma, W., Chen, C., and Zhao, J.: Photochemical Cycling of Iron

749 Mediated by Dicarboxylates: Special Effect of Malonate, Environmental Science &

750 Technology, 44, 263–268, https://doi.org/10.1021/es901956x, 2010.

751 Weller, C., Horn, S., and Herrmann, H.: Photolysis of Fe(III) carboxylato complexes: Fe(II)

752 quantum yields and reaction mechanisms, Journal of Photochemistry and Photobiology A:

753 Chemistry, 268, 24–36, https://doi.org/10.1016/j.jphotochem.2013.06.022, 2013.

754 Yuan, Y., Feng, L., Xie, N., Zhang, L., and Gong, J.: Rapid photochemical decomposition of

755 perfluorooctanoic acid mediated by a comprehensive effect of nitrogen dioxide radicals and

756 Fe^{3+}/Fe^{2+} redox cycle, Journal of Hazardous Materials, 388, 121730,

757 https://doi.org/10.1016/j.jhazmat.2019.121730, 2020.

758